NACA

RESEARCH MEMORANDUM

NACA Res. Abstracts, Aug 24, 1955

AN INVESTIGATION OF THE CHARACTERISTICS OF THE NACA RM-10

(WITH AND WITHOUT FINS) IN THE LANGLEY 11-INCH HYPERSONIC

TUNNEL AT A MACH NUMBER OF 6.9

By William D. McCauley and William V. Feller

Langley Aeronautical Laboratory
Langley Field, Va.

NATIONAL ADVISORY COMMITTEE
FOR AERONAUTICS
WASHINGTON
November 26, 1954

CONFIDENTIAL

NATIONAL ADVISORY COMMITTEE FOR AERONAUTICS

RESEARCH MEMORANDUM

AN INVESTIGATION OF THE CHARACTERISTICS OF THE NACA RM-10

(WITH AND WITHOUT FINS) IN THE LANGLEY 11-INCH HYPERSONIC

TUNNEL AT A MACH NUMBER OF 6.9

By William D. McCauley and William V. Feller

SUMMARY

The aerodynamic characteristics of a 1/12-scale model of the NACA
RM-10 have been investigated in the Langley 11-inch hypersonic tunnel
at a Mach number of 6.9. Longitudinal pressure surveys were made on
the body without fins at zero lift and at angles of attack. At zero
lift, the method of characteristics slightly underestimated the pres-
sures over the body; Van Dyke's second-order theory and the conical
shock-expansion method underestimated pressures by slightly more than
the characteristics method. Newtonian theory gives a poor estimate of
the pressures over the forebody at an angle of attack of 0°. Newtonian
impact theory and Grimminger, Williams, and Young correlation prediction
slightly underestimate the lift, drag, and pitching moment but give a
good prediction of the angle-of-attack trends.

For the lift, drag, and pitching-moment coefficients through the
angle-of-attack range of this investigation the interference effects
between the relatively large fins (span = 3 body diameters) and the body
were negligible and rotating the fins 45° from the horizontal-vertical
position had no effect.

A Mach number correlation of the data from this investigation and
other facilities indicates that, for the body alone, with increasing
Mach number, the center of pressure moved rearward, the lift-curve
slope at zero lift increased, and the skin-friction drag at zero lift
in laminar flow was essentially constant. For the finned body, as Mach
number increased the center of pressure moved forward and the lift-curve
slope at zero lift decreased.

INTRODUCTION

In order to assess the scale effects on aerodynamic characteristics
obtained from different wind tunnels and free-flight facilities, the

NACA has initiated an integrated research program on the NACA RM-10 fin-stabilized parabolic body of revolution. The results of the investigation thus far cover a Reynolds number range from about 1×10^6 up to 160×10^6 and a Mach number range from 0.85 up to 3.4 (refs. 1 to 20). The basis for correlation which has been used most frequently has been the total drag and its components at zero lift. Data at angles of attack have been correlated at Mach numbers up to 2.4 in reference 13.

The purpose of this report is to present results obtained in the Langley 11-inch hypersonic tunnel at a Mach number of 6.9 for angles of attack from 0° to about 20°, to correlate the drag components at zero lift for Mach numbers up to 6.9 at a Reynolds number of approximately 3.5×10^6, to correlate angle-of-attack effects for Mach numbers up to 6.9, and to analyze fin-body interference effects at a Mach number of 6.9.

SYMBOLS

A maximum cross-sectional area of body, sq ft

C_C chord-force coefficient, $\dfrac{\text{Chord force}}{qA}$

C_D drag coefficient, $\dfrac{\text{Drag}}{qA}$

C_L lift coefficient, $\dfrac{\text{Lift}}{qA}$

C_M pitching-moment coefficient (about the nose), $\dfrac{\text{Pitching moment}}{qAl}$

C_N normal-force coefficient, $\dfrac{\text{Normal force}}{qA}$

C.P.   center of pressure, body lengths from the nose

l length of body, ft

L/D lift-drag ratio

M free-stream Mach number

p_1 free-stream static pressure, lb/sq ft

p_2 local or body static pressure, lb/sq ft

q free-stream dynamic pressure, $\frac{\gamma}{2}p_1M^2$ or $\frac{1}{2}\rho V^2$, lb/sq ft

r radius of body at an axial station, ft

R free-stream Reynolds number, $\frac{\rho V l}{\mu}$

V free-stream velocity, ft/sec

x axial distance from body nose, ft

$\frac{x}{l}$ axial distance from body nose in body lengths

α angle of attack, deg

β cylindrical coordinate around body, deg

γ ratio of specific heats, 1.4 for air

θ cone semiapex angle, deg

ρ free-stream density, slugs/cu ft

μ coefficient of viscosity, lb-sec/ft^2

Subscripts:

b   base drag

B   body

BT   body-tail combination

f   skin-friction drag

p   pressure force (integrated from pressure distributions)

T   tail

APPARATUS AND METHODS

Tunnel

These tests were conducted in the Langley 11-inch hypersonic tunnel. Air is stored at 50 atmospheres pressure and is released through an adjustable pressure regulating valve and a new instantaneous air heater with nickel-chromium-alloy tube resistance elements (replacing the storage heater described in refs. 21 and 22) to the settling chamber and nozzle. The nozzle is a single-step two-dimensional type with a 0.1- by 10-inch throat and a 10.5- by 10-inch test section. The central core of the test section flow where all model testing done is essentially uniform over a cross section 5 inches square. Downstream of the test section is a model support strut and an adjustable double-wedge diffuser, followed by a cooler and the vacuum tanks. Details of the tunnel construction and nozzle calibration may be obtained from references 21 and 22.

Instrumentation

Force tests are made by mounting the model on a shrouded sting which is supported by a strain-gage balance. For smaller forces, a sensitive two-component balance which measured up to 5 pounds normal force and 2 pounds chord force was used. Larger forces were measured on a two-component balance which gave lift to 20 pounds and drag to 10 pounds. Pitching moments were measured on a single-component balance which read a maximum moment of 12 inch-pounds around a center forward of the balance itself. Improved estimates of the heating effects and interaction of the lift component with the drag component now exist and are accounted for in the section entitled "Data Accuracy." In addition, corrections for moment interaction were made. For a detailed description of the two-component balances, see reference 23.

Model surface pressures were recorded on film by the evacuated capsule instruments described in reference 21. The motion of a diaphragm rotates a small mirror to displace the trace of a light beam falling on a moving film. Pressure cells were chosen to give as near full-scale deflection as possible for the measuring station. The stagnation pressure was measured with Bourdon tube gages.

Schlieren System

The schlieren system used in these tests has a single-pass, vertical Z, light path with a horizontal knife edge. Film exposures were of

approximately 3 microseconds duration. The angle of attack was measured
from the schlieren film negatives to within 0.2° through the use of an
optical comparator.

Combination Fluorescent Oil and Schlieren Pictures

For visualizing the surface and exterior flow simultaneously, a
combination fluorescent oil and schlieren technique was used by coating
the finned-body force model with SAE 30 motor oil and a few spots of
graphite. The schlieren system was used with 1/50-second exposures and
with ultraviolet highlighting which caused the oil to fluoresce.

Models

The models used in this investigation are shown in figures 1 and 2.
Both models are of highly polished steel and the body diameters were
held within 0.001 inch of the values calculated from the equation for
the generating parabola. The force model had an alternate tail (figs. 1
and 2) for tests without fins.

TUNNEL CONDITIONS

During the tests the tunnel was operated at a stagnation temper-
ature of approximately $1,130°$ R and through a stagnation pressure range
from 15 to 37 atmospheres. The model Reynolds numbers (based on body
length) were in the range from approximately 1.8×10^6 to 4.5×10^6.
The length of the test runs varied from 60 to 75 seconds. The data
were evaluated at 55 seconds after the start of each run in order to
reduce the effects of a slight Mach number variation with time during
the run. Recent nozzle calibrations show that at this time during the
run the Mach number is 6.9 at a stagnation pressure of 33 atmospheres.
At a stagnation pressure of 21 atmospheres, calibrations indicate a
Mach number of 6.84 at this time while Mach numbers of 6.86 and 6.92
are indicated at stagnation pressures of 25 and 37 atmospheres,
respectively.

DATA ACCURACY

The maximum possible error in angle-of-attack measurements is 0.2°,
and in stagnation pressure is ± 5 inches mercury absolute. The maximum
possible errors in the coefficients are presented in the following table:

| | Maximum possible error, percent, for angles of attack of - | | | | | |
| | 2.5° | | 7.5° | | 12.5° | |
	With Fins	Without Fins	With Fins	Without Fins	With Fins	Without Fins
$\dfrac{\Delta C_L}{C_L}$	8	15	10	6	5	7
$\dfrac{\Delta C_D}{C_D}$	7	6	11	5	5	7
$\dfrac{\Delta C_m}{C_m}$	10	21	12	9	8	13
$\dfrac{\Delta C.P.}{l}$	2	6	1	4	1	4

Inasmuch as these errors are the maximum possible total of individual possible errors, the actual errors are probably seldom this large.

ANALYSIS AND RESULTS

Pressure Distributions

The longitudinal pressure distributions for the parabolic body of revolution are presented in figure 3 for angles of attack of 0°, 7.5°, and 15° at Reynolds numbers of approximately 4.0×10^6. The pressure model was 10.0 inches long; therefore, an extrapolation of the data to the 12.2-inch base station of the force model was necessary.

Zero lift.- At zero lift (fig. 3(a)), the experimental pressure distribution has been compared to the method of characteristics (ref. 24), Van Dyke's second-order theory (ref. 25), a conical shock two-dimensional expansion method[1] (refs. 26 and 27), linear theory (ref. 28), and Newtonian impact theory (ref. 29). The method of characteristics

---

[1]Reference 26 showed good agreement between the method of characteristics and the conical-shock expansion method on ogive noses with hypersonic similarity parameters of one or greater. The RM-10 parabolic forebody in these tests had a hypersonic similarity parameter of 0.92.

(19-point calculation) gives the best longitudinal pressure trend; it closely predicts the pressures near the nose, and then underestimates the pressures by increasing increments toward the base. Van Dyke's second-order theory also gives the appropriate trend with values not greatly different from those given by characteristics theory. The conical-shock two-dimensional expansion theory, which also gave the proper trend, started with good agreement at the nose but underestimated the pressures by a greater amount than either the method of characteristics or Van Dyke's second-order theory at rearward stations. Newtonian impact theory underestimates pressures near the nose by a greater amount than the preceding theories and predicts a pressure coefficient of zero at and behind the maximum thickness station. As would be expected, linear theory did not give a reasonable longitudinal pressure trend. It should be pointed out that the theories considered have not taken into account viscous effects. Correcting the body contour by the boundary-layer displacement thickness increases the pressure coefficients along the body length and accounts for most of the difference between the theoretical and experimental pressures.

Angle of attack.- The longitudinal pressure distributions at angles of attack of 7.5° and 15° have been compared with those predicted by Newtonian impact theory (ref. 29) in figures 3(b) and 3(c). The theory and experiment agree well on the part of the body which "sees" the flow. On the lee surfaces, the Newtonian impact theory gives a pressure coefficient of zero which appears to approach agreement with experiment as the angle of attack is increased. However, as was shown in figure 8 of reference 30 for circular cylinders at Mach number 6.9, the Newtonian impact theory predicts the normal force accurately only over a limited range of angles of attack. Hence, it cannot be assumed that the Newtonian impact theory will predict pressures accurately at angles of attack significantly above 15°.

It is interesting to note in figure 3(b) that the pressure coefficients show a minimum at $\beta = \pm 120°$ for an angle of attack of 7.5°. At $\alpha = 15°$ (fig. 3(c)) the minimum is less pronounced. A similar effect is described in reference 1 at lower Mach numbers where separation and vortex shedding were believed to occur.

Forebody Pressure Forces

The longitudinal pressure distributions at zero lift and angle of attack have been integrated to obtain force and moment coefficients. The results are tabulated on the following page:

Integration of -	α, deg	C_D	C_L	C_M	Center of pressure
Experimental data $(R = 4 \times 10^6)$	0	0.02179	------	------	-----
Method of characteristics	0	.02375	------	------	-----
Conical-shock two-dimensional expansion theory	0	.02480	------	------	-----
Van Dyke's second-order theory	0	.02230	------	------	-----
Linear theory	0	.02380	------	------	-----
Newtonian theory	0	.0120	------	------	-----
Newtonian theory	7.5	.0735	0.357	-0.1420	0.392
Newtonian theory	15	.355	1.132	-.552	.422
Experimental data $(R = 4 \times 10^6)$	7.5	.0889	.4300	-.1940	.443
Experimental data $(R = 4 \times 10^6)$	15	.3859	1.2373	-.628	.485

These values will appear for comparison purposes on the force data plots to be discussed in the following sections.

Body Forces

The experimental body force coefficients are presented in figure 4 for $R = 3.0 \times 10^6$ and $R = 4.0 \times 10^6$. The data have been compared with Newtonian impact theory (ref. 29), with Grimminger, Williams, and Young's correlation prediction (ref. 29), and with the integrated pressure data.

Lift coefficient.- The Newtonian impact theory underestimates the lift of the body (fig. 4). It was shown in figures 3(b) and 3(c) that the pressures on the windward side are predicted closely at angles of attack of $7\frac{1}{2}^\circ$ and 15° so that the discrepancy in this case may be attributed mostly to the lee side of the body where the Newtonian impact theory gives a pressure coefficient of zero. Grimminger, Williams, and Young's correlation prediction was utilized by assuming the body to consist of a conical nose, a cylindrical midbody, and a boattailed afterbody to obtain $C_{N_B} = 0.0354\alpha + 11.7 \sin^2\alpha$, and because C_{C_B} is relatively small, $C_{L_B} = (0.0354\alpha + 11.7 \sin^2\alpha)\cos \alpha$. This prediction appears to agree well with the lift data through the complete angle-of-attack range. The integrated pressure forces at 7.5° and 15° angle of attack lie within the scatter of the lift-force data and indicate good agreement between force balance and pressure results.

Drag coefficient.- The Newtonian impact theory does not include viscous effects; therefore, the calculated drag can only be compared with the pressure drag. As in the case of lift, the Newtonian impact theory underestimates drag which is again considered to be due to a pressure coefficient of zero on the expansion areas of the body surface. Grimminger, Williams, and Young's correlation prediction of C_{N_B} has been utilized in the case of drag by assuming that the variation of C_{c_B} through the angle-of-attack range can be neglected. Thus, if the experimental $C_{D_{B_{\alpha=0}}}$ is available, $C_{D_B} = C_{D_{B_{\alpha=0}}} + C_{N_B} \sin \alpha$. The prediction necessarily starts at the experimental $C_{D_{B_{\alpha=0}}}$ (fig. 4) and follows the Newtonian impact theory closely.

L/D ratio.- The L/D curve calculated by the Newtonian impact theory agrees well with the L/D ratio calculated from the integrated pressure data at angles of attack of 7.5° and 15° (fig. 4). Since the skin-friction drag is not included in the lift-drag ratio calculated from Newtonian theory, the "frictionless" L/D ratio can be expected to be much larger than the "total drag" L/D ratio at small angles of attack.

The Grimminger, Williams, and Young correlation prediction of L/D obtained by using the drag term described in the preceding section includes the friction drag at zero lift. The L/D ratio thus formed follows the trend of the force test L/D but is high through the angle-of-attack range because of the underestimation of C_{D_B}.

Fin-Body Combination Forces

The experimental fin-body combination forces are presented in figure 5. Two-dimensional shock-expansion theory for the fins and viscous effects have been added to the body-force prediction from Newtonian impact theory, to Grimminger, Williams, and Young's body correlation prediction, and to the body-alone force data for comparison with the fin-body data.

Lift coefficient.- Two-dimensional shock-expansion theory was utilized to obtain the lift of the two horizontal fins. To this lift, a correction was applied for the region of the fins lying in the tip Mach cone. The assumption made was that suggested by Lighthill (ref. 31) that the area of the wing in the tip Mach cone has an average pressure one-half that of the two-dimensional region of the wing. The net effect decreases the shock-expansion fin-lift contribution by approximately 4 percent. The fin lift was then added to the Newtonian impact body theory, the Grimminger, Williams and Young body correlation prediction, and the body data. When the shock-expansion theory was

computed on the fins, it was necessary to discontinue calculations above approximately an angle of attack of 12.5° because the leading-edge shock became detached at that point. The curves appearing in figure 5 have been extrapolated up to 15° beyond which extrapolation did not appear to be warranted.

The body data plus two-dimensional shock-expansion theory for the fins gave good agreement with the C_L data for the finned body. Grimminger, Williams, and Young's correlation prediction slightly over-estimates the C_L data and the Newtonian theory slightly underestimates C_L data. The agreement of experimental data with all three theories can be considered satisfactory.

The solid data points in figure 5 give the effects of positioning the fins at 45° roll from the horizontal-vertical position. Within the scatter of the data no effects have been observed in the lift; this result tends to substantiate the prediction of linear theory as obtained by Spreiter (ref. 32).

Figure 6 has been prepared to indicate the interference effects on the fins. Figure 6(a) shows the difference between the experimental lift of the fin-body combination and the body alone compared with the lift obtained by the shock-expansion theory for the fins. Figure 6(b) indicates the proportion of the lift of the body-tail combination which is due to the fins. The shock-expansion theory lies slightly above the average of the data but within the scatter over the angle-of-attack range. Reference 23 indicates a similar overestimation of theory over experiment due in part to flow separation on the upper wing surfaces. The assumption of two-dimensional flow over the fins seems to be justi-fied because the interference effects are obviously small.

Drag coefficient.- Two-dimensional shock-expansion theory with tip correction was also utilized for the fin pressure drag. In order to facilitate the computation, it was assumed that the two horizontal fins were acting at angles of attack and that the two vertical fins were contributing zero lift drag. This assumption is not strictly true because the lower vertical fin is sweeping forward as the angle of attack increases whereas the upper vertical fin sweeps rearward. The situation is further complicated by the fact that at an angle of attack of approximately 7° the top vertical fin is completely blanketed by the body wake. The sweep effects are partially compensating and the top vertical fin in its worst condition (approximately 7°) contributes only 2.6° percent of the drag so that the sweep and blanketing effects on the vertical fins are considered to be negligible. A simple estimate of the skin-friction drag on the fins was obtained from Bertram (ref. 33)

by assuming the fins to be flat plates with pressure gradients. This estimate is

$$c_{D_{fT}} = \frac{140}{\sqrt{R_B}}$$

The fin pressure and skin-friction drags were added directly to the Grimminger, Williams, and Young correlation prediction and to the faired body force data. For the integrated body pressure data and the Newtonian body forces, it was also necessary to add an estimated body skin friction. Inasmuch as the boundary layer at zero lift was observed to be laminar, the estimated body skin friction was obtained from the Blasius relation (with the Topfer constant) for a flat plate with zero pressure gradient and zero heat transfer. Mangler's transformation (ref. 34) was utilized to convert these values to those for a body of revolution; for the RM-10 body it increased the flat-plate values 6 percent. Using then the ratio of surface area to cross-sectional area, one obtains

$$c_{D_{f_B}} = \frac{51.2}{\sqrt{R_B}}$$

In figure 5, the experimental $c_{D_{BT}}$ from force data for the finned body agrees well with the body data with fin effects added. The Grimminger, Williams, and Young correlation prediction with fin effects underestimates with increasing angle of attack in the same manner as it did for the body-alone data. The Newtonian theory and the integrated body pressure data, which have the fin effects and body skin friction added, appear to underestimate the data. If the integrated body pressure data had the proper amounts of fin effects and skin-friction drag added, it should agree with the finned-body data. Inasmuch as the estimation of the skin-friction drag of the fin appears to be correct, the skin-friction drag of the body has evidently been underestimated.

L/D ratio.- The maximum L/D from the finned-body force tests is 3.31 at an angle of attack of 8° (fig. 5). The theoretical lift-drag ratio for the body data with fin effect added agrees with the finned-body force data except at small angles of attack where possible data uncertainties in lift and drag are. magnified in their ratio.

The lift-drag ratio obtained from the Newtonian impact theory, as in the case of the body-alone data, agrees with the pressure data. This result is not surprising because the same fin effects and skin-friction drags have been added to each. The maximum L/D occurs at $\alpha = 7°$.

The Grimminger, Williams, and Young correlation prediction $(L/D)_{max} = 3.82$ at $\alpha = 8^\circ$ is slightly high; this effect is probably due to neglecting changes in chord force with angle of attack.

Pitching Moment and Center of Pressure

The pitching moments and centers of pressure of the body alone and the body with fins are presented in figure 7. The body-alone data are compared with the Newtonian impact theory and the data for the body with fins are compared with the combined Newtonian impact theory for the body and the two-dimensional shock-expansion theory for the fin.

Body alone.- The Newtonian impact theory section forces were integrated over the body length to obtain the center of pressure and pitching moment of the body alone. In figure 7, the variation in center of pressure for the body alone with increase in angle of attack exhibits the same trend as at lower Mach numbers (refs. 2, 12, and 13); the center of pressure moves rearward as angle of attack increases. The Newtonian impact theory gives a reasonable estimate of center of pressure of the body alone at all angles of attack, although it gives values which are too far forward near $\alpha = 0^\circ$. This is due to the fact that, at small angles, the pressure coefficient on the lee side of the body is equal to zero. This condition was shown in figures 3(a), 3(b), and 3(c) to represent the conditions adequately at $\alpha = 7.5^\circ$ and 15° but not at $\alpha = 0$. The body pitching moments are underestimated by Newtonian theory through the complete angle-of-attack range. This result seems reasonable if the underestimation is attributed to C_{N_B} which was the principal contributor to a low C_{L_B}.

Body with fins.- The two-dimensional shock-expansion C_{N_T} values were summed to calculate the normal force and moment due to the tail and were added to those of the Newtonian body theory to obtain an estimate of the finned-body pitching moment and center of pressure. The finned-body center of pressure appeared to be constant (within the data scatter) at 0.67 body lengths from the nose for the range of angle of attack in which these data were obtained. The combined theory also predicts a constant center of pressure for the fin-body combination at approximately 0.71 body lengths from the nose. This type of angle-of-attack trend also occurred at lower Mach numbers (refs. 2 and 13) on the finned-body combination. For the fin-body combination the agreement between the theoretical and experimental pitching-moment data is good, even though the Newtonian impact theory underestimated the body normal force, because the fins, for which good estimates of the normal force are available, contribute about one-half the normal force of the total configuration and most of the moment.

Spreiter (ref. 32) has shown through the use of linear theory that the pitching moments of a finned body at small angles of attack are unaffected by roll position. This investigation appears to confirm this conclusion as have other investigations by Grigsby and Rainey (refs. 35 and 36) at lower Mach numbers. The pitching-moment data have been obtained for two roll conditions, the fins vertical and horizontal and rotated 45°; no change was noted due to different roll positions.

Variation of the Zero-Lift Drag Components

With Reynolds Number

The body and finned body were tested at zero lift through a range of Reynolds numbers at constant temperature by varying the stagnation pressure from approximately 15 to 37 atmospheres. The results are presented in figure 8 with the base pressure, integrated body pressure drag, fin pressure drag by shock-expansion theory, and estimated skin frictions for the body and fins in order to compare the sum of the calculated drags with the measured values. The base-pressure drag is less than 0.1 percent of the finned-body total drag. The integrated body pressure drag obtained at $R = 3.96 \times 10^6$ which has been assumed constant over the Reynolds number range was about 21 percent of the total drag. The estimated body skin friction varied from approximately 28 percent of the total drag at $R = 2 \times 10^6$ to 23 percent at $R = 4.5 \times 10^6$. A curve has been faired through the data for the body so that, with the restriction of constant body pressure drag for various Reynolds numbers, the blank space between the shaded estimated body skin friction and the faired body data indicates the error in the estimated body skin friction. The fin pressure drag from the shock-expansion method, when added to the faired body data, contributed 14 to 17 percent of the total drag in the range of test Reynolds numbers. The estimated skin friction of the fin contributed 34 to 39 percent of the total fin body drag in the same Reynolds number range. The small blank area between the shaded estimated skin friction of the fin and the faired fin-body data indicated that interference effects are small.

Variation of the Zero-Lift Drag Components

With Mach Number for the Body Alone

A Mach number correlation of the zero-lift drag components for the body alone is presented in figure 9. The abscissa used here is the reciprocal of the Mach number. Since the boundary layer at Mach number 6.9 was laminar, it was necessary to select similar laminar-flow data

at lower Mach numbers. Fortunately, laminar-flow data at comparable
Reynolds numbers were available from the investigations of references 7
and 11 and are included in this correlation.

From figure 9 the base-pressure drags at Mach numbers down to
$M = 1.6$ ($1/M = 0.625$) appear to fair into a single curve, whereas the
base-pressure drag from the investigation in the Langley 4- by 4-foot
supersonic pressure tunnel (ref. 7) has large scatter and seems to fair
to an entirely different curve. This particular model and data are
discussed by Love, Coletti, and Bromm (ref. 11) and the results are
considered to be the effects of wake transition; thus, the faired curve
below $1/M = 0.625$ ($M = 1.6$) would be considered to be a laminar wake
whereas the data from the Langley 4- by 4-foot tunnel would be a
turbulent wake. The integrated forebody pressure drag from the three
facilities is presented and compared with Lighthill's second-order
theory as applied in reference 11 up to Mach number 4 which is the
extreme limit of applicability of this theory to this body. This
curve is extrapolated beyond Lighthill's prediction at $M = 4$,
faired through the method of characteristics value at $M = 6.9$ and
into the Newtonian theory value at $M = \infty$. Next, a prediction was
obtained by the method of Fraenkel; reference 37, in which character-
istic results at low Mach numbers for various parabolic forebodies and
parabolic afterbodies are plotted against the hypersonic similarity
parameters. It would be difficult to choose between the predictions
of Lighthill's and Fraenkel's theories because in the range of Mach
numbers for which data are available there is not a great deal of
difference between them and both can be considered to give a good
representation of the experimental results.

The body skin friction was obtained by subtracting the base and
pressure drags from the total force drag on the body. An average
curve has been drawn through the test data and it will be noticed that
this curve indicates almost a constant value (0.029) of skin friction
over the complete Mach number range.

Because of the different base pressure drags, it was considered
advisable to plot the total or force drags minus the respective base
drags. These are compared with the pressure drags of Lighthill
(extended through the characteristics point at $M = 6.9$) and Fraenkel
which have a value of skin friction of 0.029 added to them. As in the
case of pressure drags, both curves seem to average the data.

Variation of Lift-Curve Slope at

Zero Lift with Mach Number

The lift-curve-slope values at zero lift from four facilities at
seven Mach numbers (refs. 2, 12, and 13) are presented in figure 10 and

are plotted against reciprocal Mach number, the faired curves indicating the probable intermediate values. For the body alone and for the finned body, the lift curve was generally nonlinear at all Mach numbers tested, being linear up to approximately 1° and 2°, respectively, and then increasing in slope with angle of attack.

In general, this figure indicates the increase in body contribution to the lift-curve slope for the fin-body combination and the decrease in fin effectiveness with increasing Mach number.

Variation of Center of Pressure

with Mach Number

The centers of pressure for the finned body and body alone are presented in figure 11 and are correlated with those from references 2, 12, and 13. For the body alone, large rearward shifts in center of pressure occur with increases in angle of attack, especially at the lower supersonic Mach numbers. For a given angle of attack the center of pressure moves rearward as Mach number is increased. The center of pressure for the body alone is forward of the 0.5 body length station for all Mach numbers.

For the finned body, the changes in center of pressure with angle of attack, for the present tests, were small for the range of angle of attack in which these data were obtained (1.2° to 13°). The centers of pressure from the data from the Lewis 8- by 6-foot tunnel (ref. 2) were approximately constant for angles of attack down to 2° (a variation not more than the height of the symbol used for the data in fig. 11). The data from the Langley 9-inch supersonic tunnel (ref. 13) which included angles of attack down to 1° indicated that a slight forward shift in center of pressure might be expected as $\alpha = 0$ is approached. The center of pressure moved forward from 0.85 body lengths to 0.68 body lengths as Mach number increased from 1.49 to 6.9. The reason for the forward shift in center of pressure for the finned body with increasing Mach number can be accounted for by an examination of figure 10 which indicates the relative decrease in fin effectiveness with increase in Mach number.

Schlieren Observations

The shock and expansion patterns and boundary-layer phenomena are shown in the schlieren pictures (fig. 12). At zero lift, a relatively thick laminar boundary lies along the complete length of the body. The bow-shock-wave half angle is 9.9° as compared with the free-stream Mach angle of 8.3°. The shocks which appear to be originating at the

base of the model actually originate at the leading edge of the hori-
zontal fins. Ahead and downstream of the bow shock, disturbances
parallel to the bow shock at $\alpha = 0°$ can be seen. Inasmuch as these
disturbances remained unchanged as the angle of attack of the model
increased, they were considered to be sidewall effects.

As the angle of attack is increased, the laminar boundary layer
on the lower surface becomes thinner while on the top surface it becomes
thicker forward and disappears from most of the body upper surface where
it is separated. On some pictures, disturbances can be seen parallel
to the undisturbed flow which might be vortices shed from the body.
Unfortunately, they cannot be resolved clearly enough to be certain.
The bow shock on the lower surface moves in close to the body contour
as α increases and possibly causes shock boundary-layer interaction
at the nose. The additional shock at the fin trailing edge at $\alpha = 17°$
is created by the intersection of the bow shock and the shock from the
vertical fin.

<p style="text-align:center">Combination Fluorescent Oil</p>

<p style="text-align:center">and Schlieren Pictures</p>

A combination fluorescent oil and schlieren technique is presented
in figure 13. The turbulent region on the left of these pictures was
caused by the heat from the ultraviolet lamp outside the tunnel and is
not part of the flow phenomena.

With this method, the boundary layer, shock waves, high and low
shear areas, and separation regions could be observed. In the side
view, an oil buildup (low shear region) is noted along the body length
separating the high shear flow on the bottom from a high shear region
near the top. From the top view, the upper high shear region noted on
the side view can clearly be seen to consist of two regions, one on
either side separated by an oil buildup in the center. These two high
shear regions on the top sides are probably due to the scrubbing action
of shed vortices.

On the horizontal fins, two separated regions can be seen. One
region, triangular in shape, starts at the junction of the fin leading
edge with the body and is due to the disturbance of the body boundary
layer by the fin. The outside edge of this region is probably defined
by a shock from the body boundary-layer disturbance. The second
separated region, which merges into the first, is the ordinary separa-
tion from the upper surface at angles of attack and remains at about
70 percent chord nearly to the tip, where it sweeps back more sharply.
The upper vertical fin also had a small separated area while the lower

vertical fin was a high shear region. It is unfortunate that, in these pictures, flow directions of the various regions could not be definitely established.

CONCLUSIONS

The aerodynamic characteristics of the NACA RM-10 parabolic body of revolution (with and without fins) were investigated in the Langley 11-inch hypersonic tunnel at a Mach number of 6.9 and Reynolds number from approximately 2.0×10^6 to 4.5×10^6. These data have been correlated with data from previous investigations at lower Mach numbers and various Reynolds numbers. From the investigation, the following results were obtained:

(1) At zero lift the method of characteristics slightly under-estimates the pressures over the body at a Mach number of 6.9. Both Van Dyke's second-order theory and the conical shock two-dimensional expansion method underestimate pressures by slightly more than does the characteristics method. Newtonian impact theory gives a poor estimate of the pressures over the forebody at $\alpha = 0^\circ$.

(2) Newtonian impact theory and the Grimminger, Williams, and Young correlation prediction both underestimate lift and drag but give a good prediction of the angle-of-attack trend for the body forces and pitching moment.

(3) For lift, drag, and pitching-moment coefficients with these relatively large span fins (3 body diameters), the interference effects at a Mach number of 6.9 over the angle-of-attack range of this investigation are small, and the total longitudinal forces and moments may be considered as a simple summation of the independent body and fin forces and moments.

(4) Rotating the fins 45° from the horizontal-vertical position had a negligible effect on lift, drag, and pitching-moment coefficients of the finned-body for angles of attack up to 10°.

(5) For the body alone at all angles of attack in the range investigated, the center of pressure moves rearward with an increase in Mach number. The rearward shifting of the center of pressure with increasing angle of attack becomes less as the Mach number increases. The center of pressure of the finned body moved forward from 0.86 body lengths from the nose at a Mach number of 1.49 to 0.68 body lengths from the nose at a Mach number of 6.9 and, in general, exhibited no shift with angle of attack for the experimental angle-of-attack range.

(6) The lift-curve slope at zero lift for the fin-body combination decreases with increasing Mach number whereas that of the body alone increases. These relative changes indicate a large decrease in fin effectiveness with increasing Mach number which causes the center of pressure to move forward on the fin-body combination with increasing Mach number.

(7) The components of drag coefficient at zero lift had the following variations as the Mach number increased from 1.40 to 6.9 at a Reynolds number of 3.4×10^6: the base drag coefficient decreased, the pressure drag coefficient decreased, and the skin-friction drag coefficient remained essentially constant; thus, the total drag coefficient decreased.

Langley Aeronautical Laboratory,
        National Advisory Committee for Aeronautics,
                Langley Field, Va., August 20, 1954.

REFERENCES

1. Luidens, Roger W., and Simon, Paul C.: Aerodynamic Characteristics of NACA RM-10 Missile in 8- by 6-Foot Supersonic Wind Tunnel at Mach Numbers from 1.49 to 1.98. I - Presentation and Analysis of Pressure Measurements (Stabilizing Fins Removed). NACA RM E50D10, 1950.

2. Essenwein, Fred T., Obery, Leonard J., and Schueller, Carl F.: Aerodynamic Characteristics of NACA RM-10 Missile in 8- by 6-Foot Supersonic Wind Tunnel at Mach Numbers From 1.49 to 1.98. II - Presentation and Analysis of Force Measurements. NACA RM E50D28, 1950.

3. Jackson, H. Herbert, Rumsey, Charles B., and Chauvin, Leo T.: Flight Measurements of Drag and Base Pressure of a Fin-Stabilized Parabolic Body of Revolution (NACA RM-10) at Different Reynolds Numbers and at Mach Numbers From 0.9 to 3.3. NACA RM L50G24, 1950.

4. Luidens, Roger W., and Simon, Paul C.: Aerodynamic Characteristics of NACA RM-10 Missile in 8- by 6-Foot Supersonic Wind Tunnel at Mach Numbers From 1.49 to 1.98. III - Analysis of Force Distribution at Angle of Attack (Stabilizing Fins Removed). NACA RM E50I19, 1950.

5. Chauvin, Leo T., and deMoraes, Carlos A.: Correlation of Supersonic Convective Heat-Transfer Coefficients From Measurements of the Skin Temperature of a Parabolic Body of Revolution (NACA RM-10). NACA RM L51A18, 1951.

6. Rumsey, Charles B., and Loposer, J. Dan: Average Skin-Friction Coefficients From Boundary-Layer Measurements in Flight on a Parabolic Body of Revolution (NACA RM-10) at Supersonic Speeds and at Large Reynolds Numbers. NACA RM L51B12, 1951.

7. Hasel, Lowell E., Sinclair, Archibald R., and Hamilton, Clyde V.: Preliminary Investigation of the Drag Characteristics of the NACA RM-10 Missile at Mach Numbers of 1.40 and 1.59 in the Langley 4- by 4-Foot Supersonic Tunnel. NACA RM L52A14, 1952.

8. Jackson, H. Herbert: Flight Measurements of the Effects of Surface Condition on the Supersonic Drag of Fin-Stabilized Parabolic Bodies of Revolution. NACA RM L52B26, 1952.

9. Czarnecki, K. R., and Marte, Jack E.: Skin-Friction Drag and Boundary-Layer Transition on a Parabolic Body of Revolution (NACA RM-10) at a Mach Number of 1.6 in the Langley 4- by 4-Foot Supersonic Pressure Tunnel. NACA RM L52C24, 1952.

10. Czarnecki, K. R., and Sinclair, Archibald R.: Preliminary Investi-
       gation of the Effects of Heat Transfer on Boundary-Layer Transi-
       tion on a Parabolic Body of Revolution (NACA RM-10) at a Mach
       Number of 1.61. NACA TN 3165, 1954. (Supersedes NACA RM L52E29a.)

11. Love, Eugene S., Coletti, Donald E., and Bromm, August F., Jr.:
       Investigation of the Variation With Reynolds Number of the Base,
       Wave, and Skin-Friction Drag of a Parabolic Body of Revolution
       (NACA RM-10) at Mach Numbers of 1.62, 1.93, and 2.41 in the
       Langley 9-Inch Supersonic Tunnel. NACA RM L52H21, 1952.

12. Cooper, Morton, Gapcynski, John P., and Hasel, Lowell E.: A Pressure
       Distribution Investigation of a Fineness-Ratio-12.2 Parabolic Body
       of Revolution (NACA RM-10) at M = 1.59 and Angles of Attack up
       to 36°. NACA RM L52G14a, 1952.

13. Coletti, Donald E.: Investigation of the Aerodynamic Characteristics
       of the NACA RM-10 Missile (With Fins) at a Mach Number of 1.62 in
       the Langley 9-Inch Supersonic Tunnel. NACA RM L52J23a, 1952.

14. Mottard, Elmo J., and Loposer, J. Dan: Average Skin-Friction Drag
       Coefficients From Tank Tests of a Parabolic Body of Revolution
       (NACA RM-10). NACA TN 2854, 1953.

15. Evans, Albert J.: The Zero-Lift Drag of a Slender Body of Revolu-
       tion (NACA RM-10 Research Model) As Determined From Tests in
       Several Wind Tunnels and in Flight at Supersonic Speeds. NACA
       TN 2944, 1953.

16. Nicolaides, John D., and Karpov, B. G.: On the Free Flight Drag
       Determination of a Finned Configuration (RM-10) Flying at Critical
       Reynolds Numbers. Memo. Rep. No. 751, Ballistic Res. Labs.,
       Aberdeen Proving Ground, Dec. 1953.

17. Maloney, Joseph P.: Drag and Heat Transfer on a Parabolic Body of
       Revolution (NACA RM-10) in Free Flight to Mach Number 2 With Both
       Constant and Varying Reynolds Number and Heating Effects on
       Turbulent Skin Friction. NACA RM L54D06, 1954.

18. Carros, Robert J., and James, Carlton S.: Some New Drag Data on
       the NACA RM-10 Missile and a Correlation of the Existing Drag
       Measurements at M = 1.6 and 3.0. NACA TN 3171, 1954.

19. Loposer, J. Dan, and Rumsey, Charles B.: Flight Measurements of
       Average Skin-Friction Coefficients on a Parabolic Body of Revo-
       lution (NACA RM-10) at Mach Numbers From 1.0 to 3.7. NACA
       RM L54G14, 1954.

20. Piland, Robert O.: Drag Measurements on a 1/6-Scale Finless Sting-Mounted NACA RM-10 Missile in Flight at Mach Numbers from 1.1 to 4.04 Showing Some Reynolds Number and Heating Effects. NACA RM L54H09, 1954.

21. McLellan, Charles H., Williams, Thomas W., and Bertram, Mitchel H.: Investigation of a Two-Step Nozzle in the Langley 11-Inch Hypersonic Tunnel. NACA TN 2171, 1950.

22. McLellan, Charles H., Williams, Thomas W., and Beckwith, Ivan E.: Investigation of the Flow Through a Single-Stage Two-Dimensional Nozzle in the Langley 11-Inch Hypersonic Tunnel. NACA TN 2223, 1950.

23. McLellan, Charles H., Bertram, Mitchel H., and Moore, John A.: An Investigation of Four Wings of Square Plan Form at a Mach Number of 6.86 in the Langley 11-Inch Hypersonic Tunnel. NACA RM L51D17, 1951.

24. Ferri, Antonio: Elements of Aerodynamics of Supersonic Flows. The Macmillan Co., 1949, pp. 261-291.

25. Van Dyke, Milton D.: Practical Calculation of Second-Order Supersonic Flow Past Nonlifting Bodies of Revolution. NACA TN 2744, 1952.

26. Eggers, A. J., Jr., and Savin, Raymond C.: Approximate Methods for Calculating the Flow About Nonlifting Bodies of Revolution at High Supersonic Airspeeds. NACA TN 2579, 1951.

27. Staff of the Computing Section, Center of Analysis (Under Direction of Zdeněk Kopal): Tables of Supersonic Flow Around Cones. Tech. Rep. No. 1, M.I.T., 1947.

28. Miles, Edward R. C.: Supersonic Aerodynamics. McGraw-Hill Book Co., Inc., 1950, pp. 127-138.

29. Grimminger, G., Williams, E. P., and Young, G. B. W.: Lift on Inclined Bodies of Revolution in Hypersonic Flow. Jour. Aero. Sci., vol. 17, no. 11, Nov. 1950, pp. 675-690.

30. Penland, Jim A.: Aerodynamic Characteristics of a Circular Cylinder at Mach Number 6.86 and Angles of Attack up to 90°. NACA RM L54A14, 1954.

31. Lighthill, M. J.: The Supersonic Theory of Wings of Finite Span. R. & M. No. 2001, British A.R.C., 1944.

32. Spreiter, John R.: Aerodynamic Forces on Slender Plane- and
    Cruciform-Wing and Body Combinations. NACA Rep. 962, 1950.
    (Supersedes NACA TN's 1897 and 1662.)

33. Bertram, Mitchel H.: An Approximate Method for Determining the
    Displacement Effects and Viscous Drag of Laminar Boundary Layers
    in Two-Dimensional Hypersonic Flow. NACA TN 2773, 1952.

34. Mangler, W.: Boundary Layers With Symmetrical Airflow About Bodies
    of Revolution. Rep. No. R-30-18, Part 20, Goodyear Aircraft Corp.,
    Mar. 6, 1946.

35. Grigsby, Carl E.: Tests at Mach Number 1.62 of a Series of Missile
    Configurations Having Tandem Cruciform Lifting Surfaces. NACA
    RM L51J15, 1952.

36. Rainey, Robert W.: An Investigation of Several Supersonic Missile
    Configurations Directed Toward Minimizing Center-of-Pressure
    Travel. NACA RM L52G01, 1952.

37. Fraenkel, L. E.: Curves for Estimating the Wave Drag of Some Bodies
    of Revolution, Based on Exact and Approximate Theories.
    C.P. No. 136 (15,685), British A.R.C., 1953.
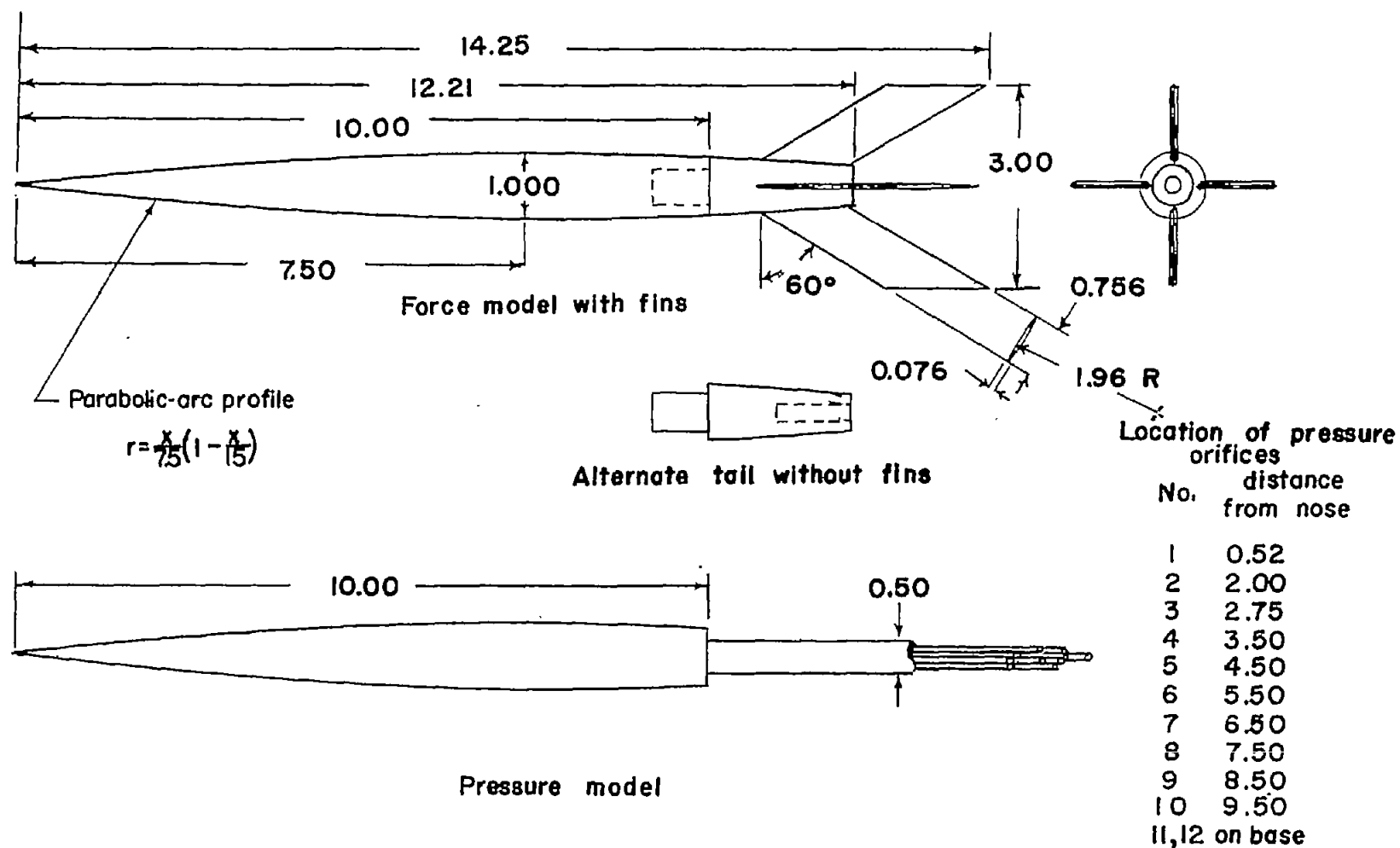
Figure 1.- NACA RM-10 models, 1/12th scale. All dimensions are in inches.
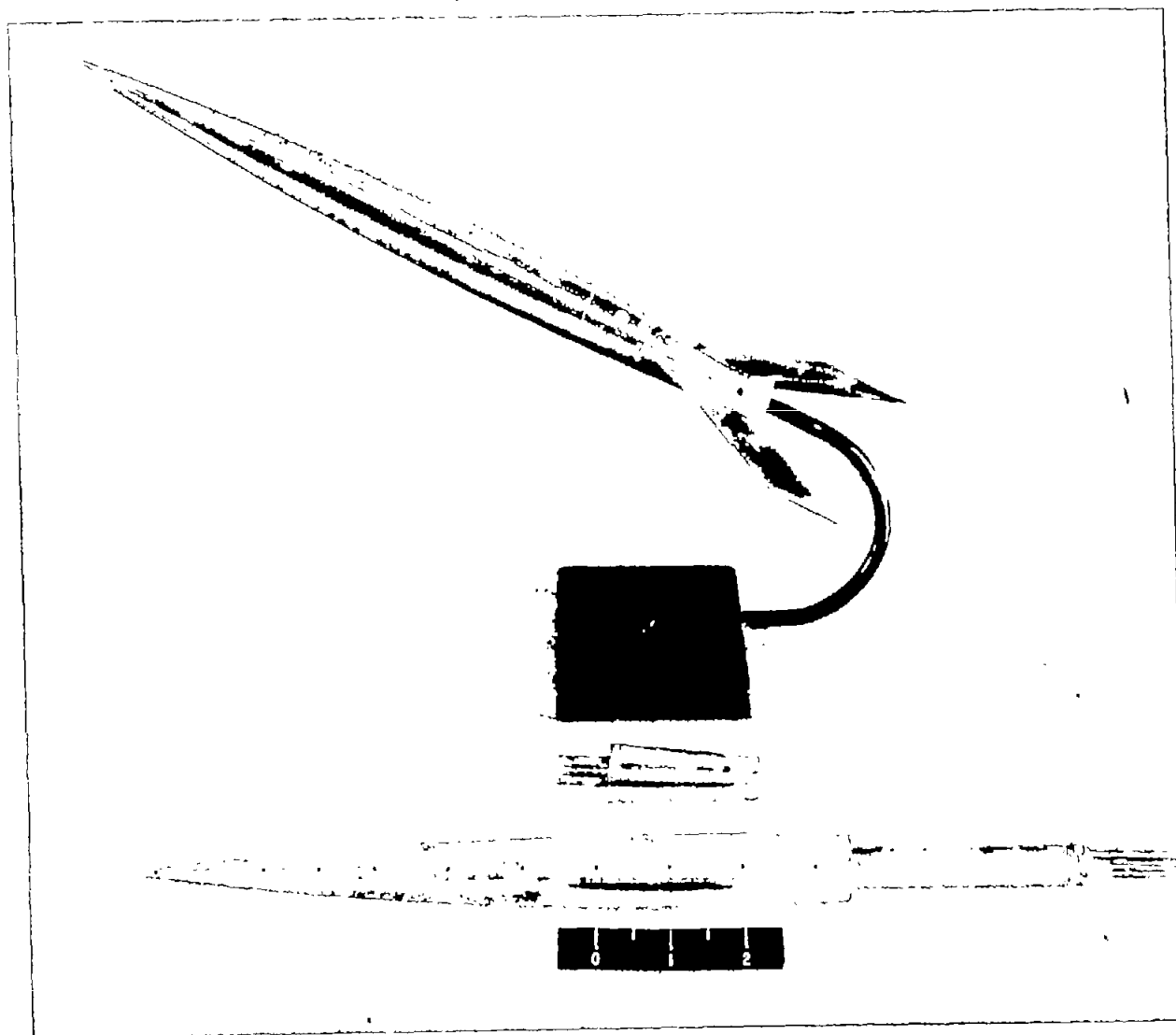
Figure 2.- Photograph of NACA RM-10 models.

L-84053

(a) Body alone; angle of attack, 0°.
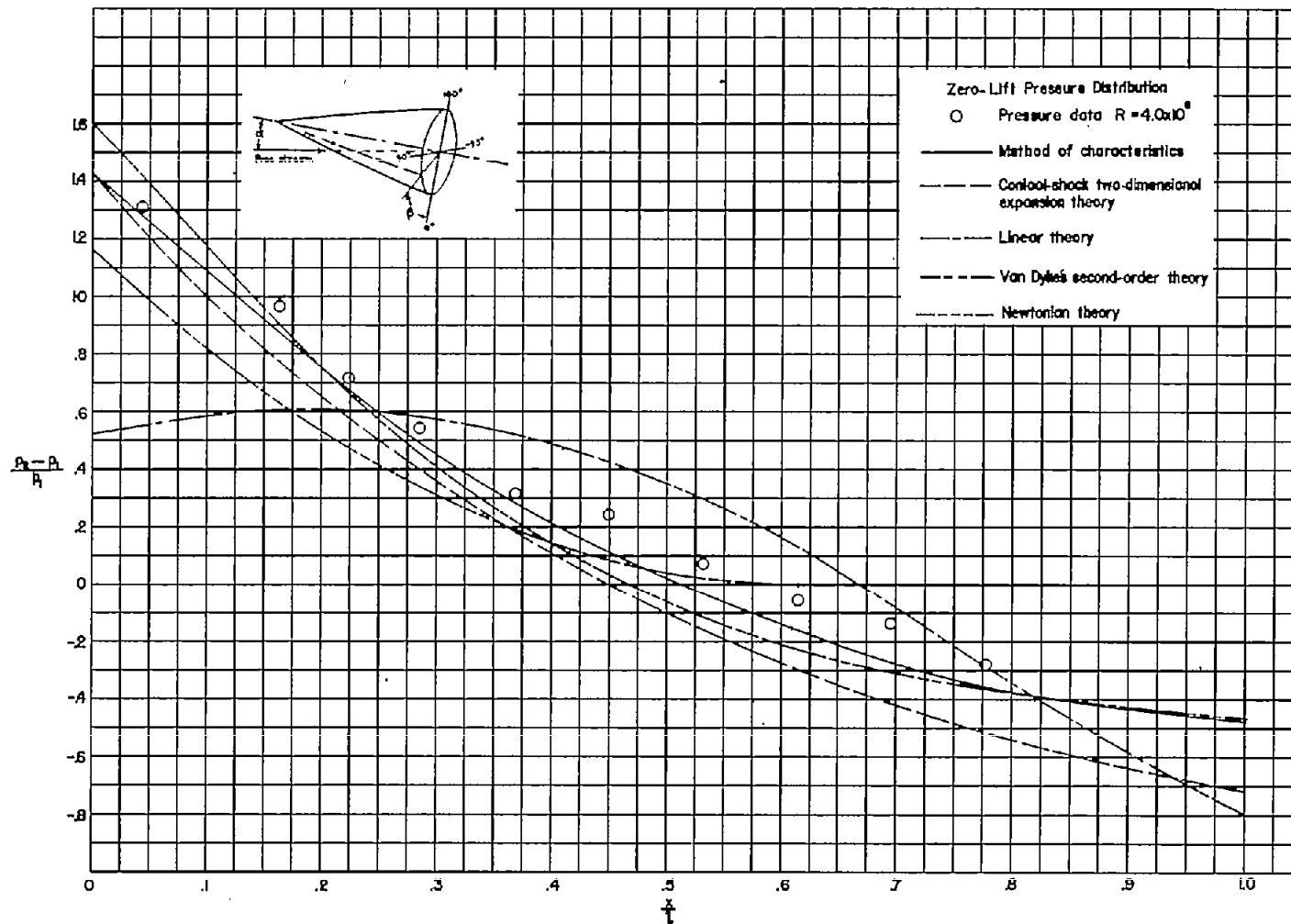
Figure 3.- Longitudinal pressure distributions at a Mach number of 6.9.
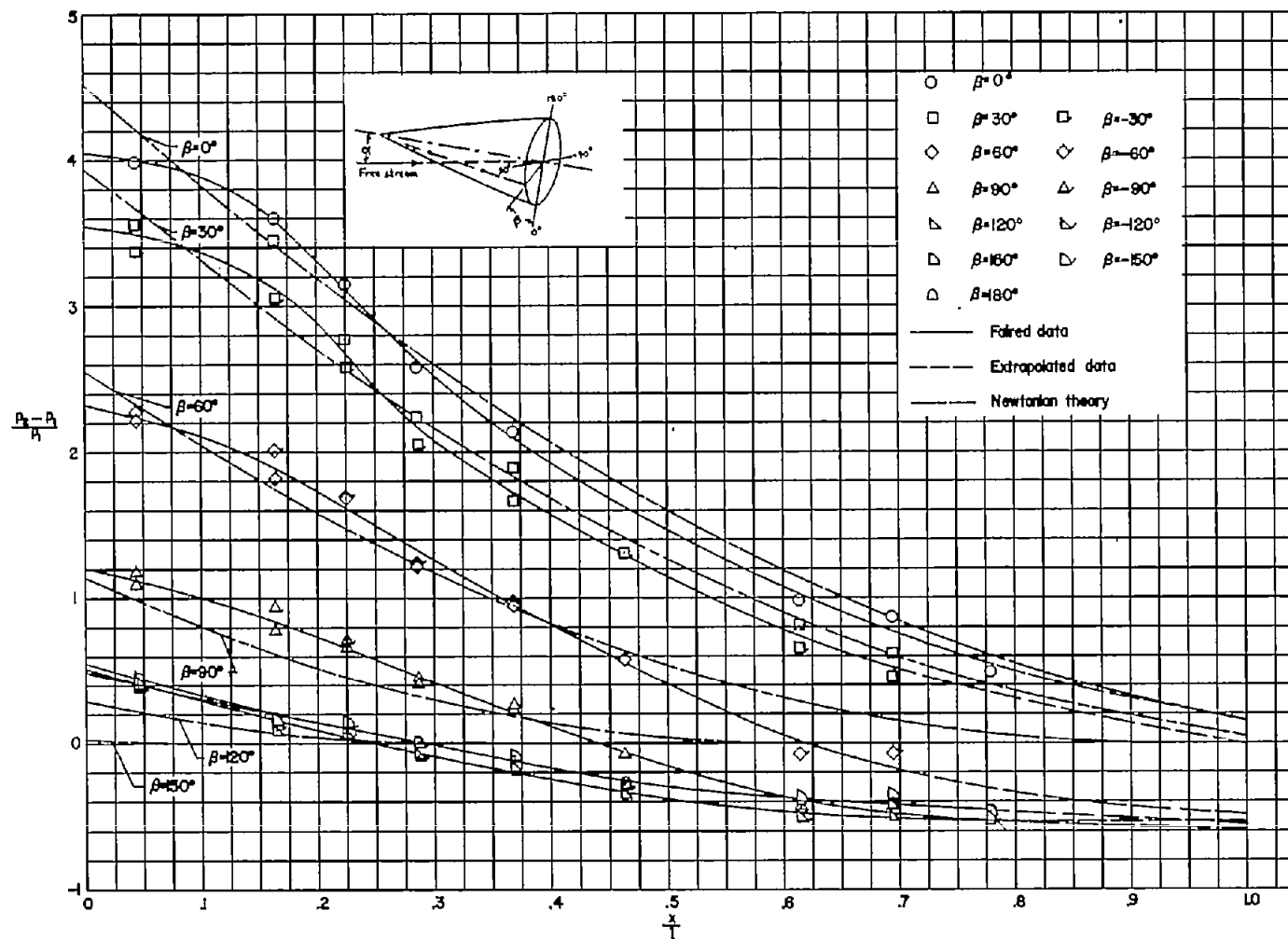
(b) Body alone; angle of attack, 7.5°.

Figure 3.- Continued.
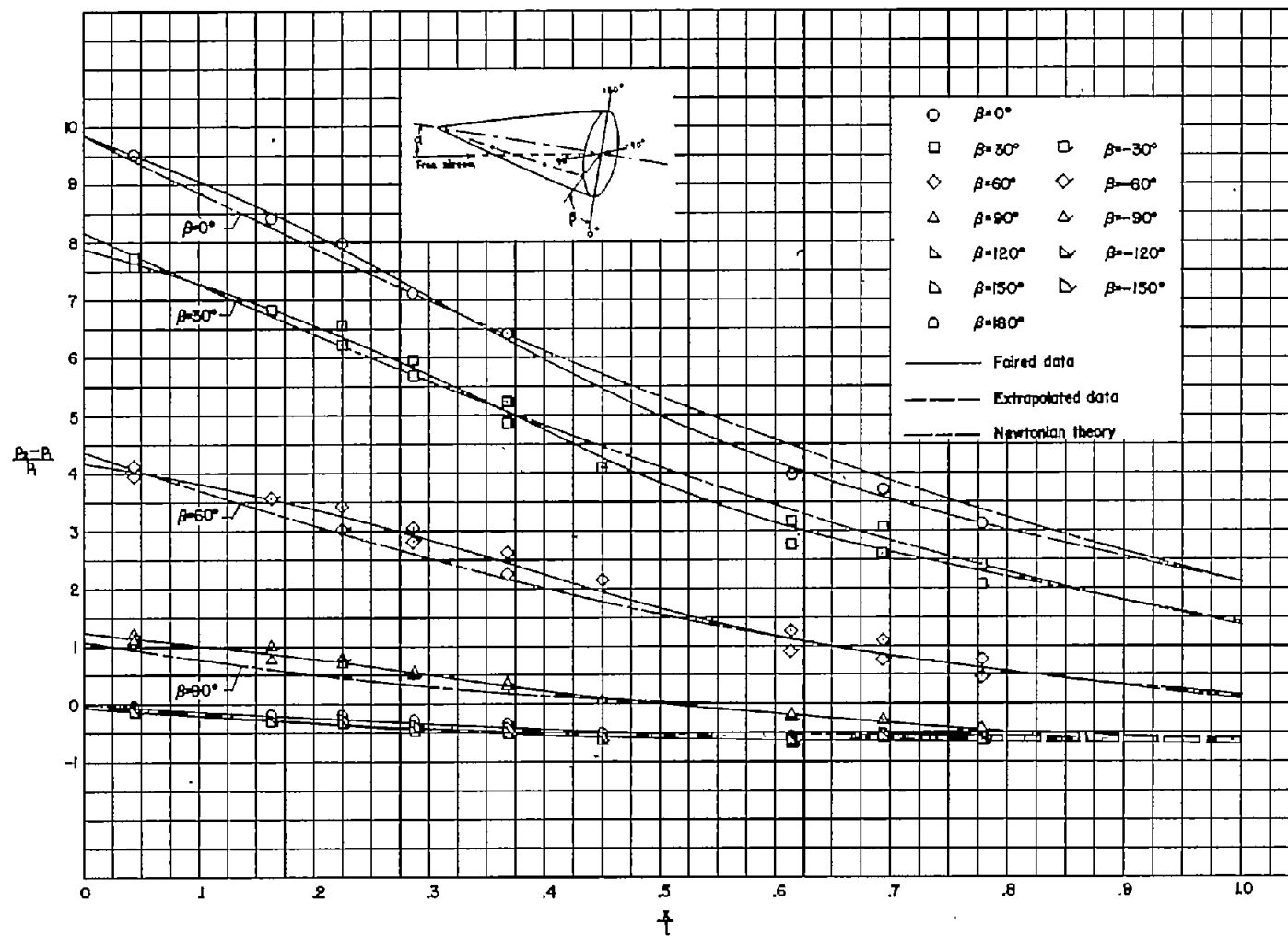
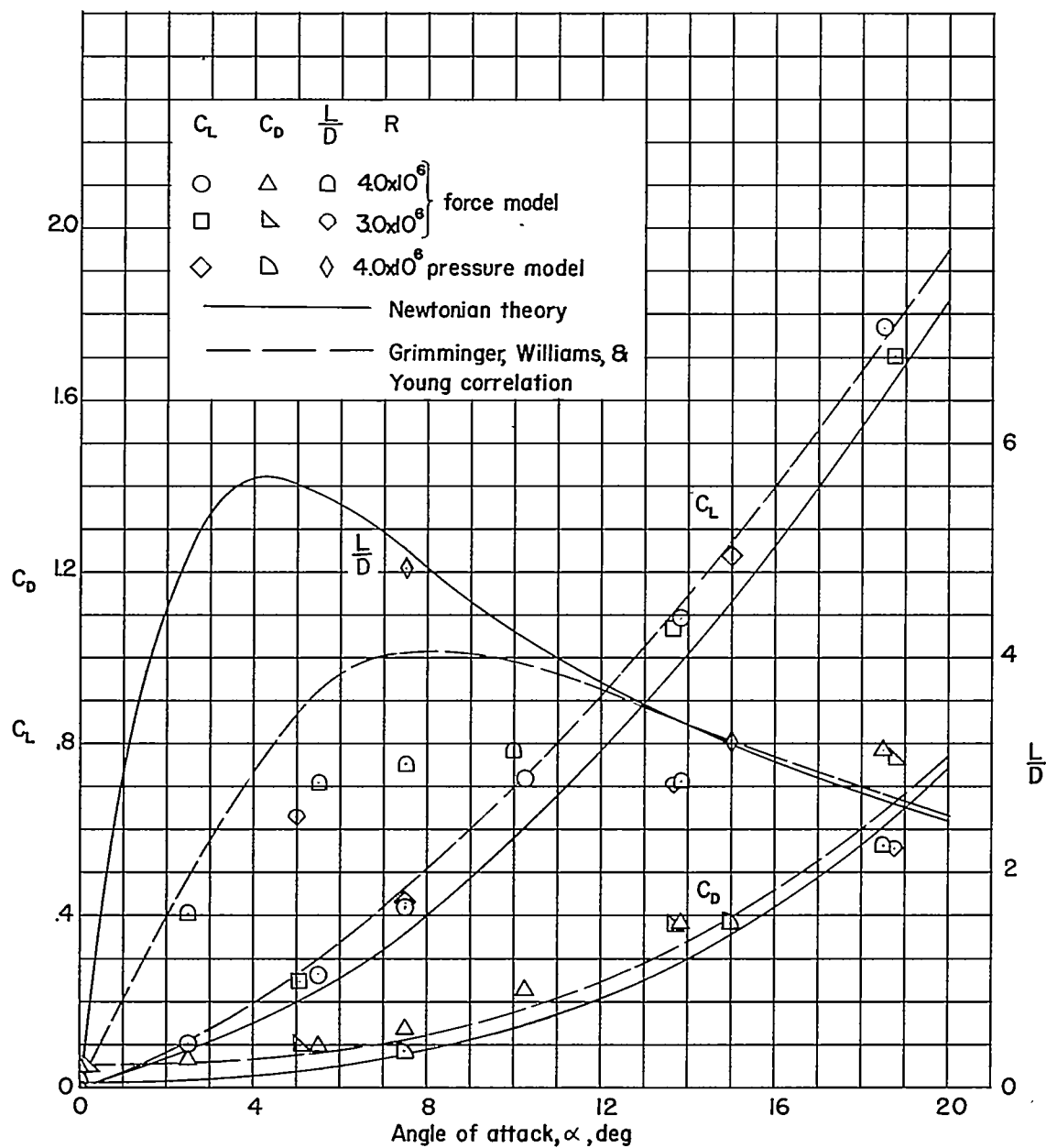(c) Body alone; angle of attack, 15°.

Figure 3.- Concluded.

Figure 4.- Experimental and theoretical variation of lift coefficient, drag coefficient, and lift-drag ratio with angle of attack for body alone at a Mach number of 6.9.
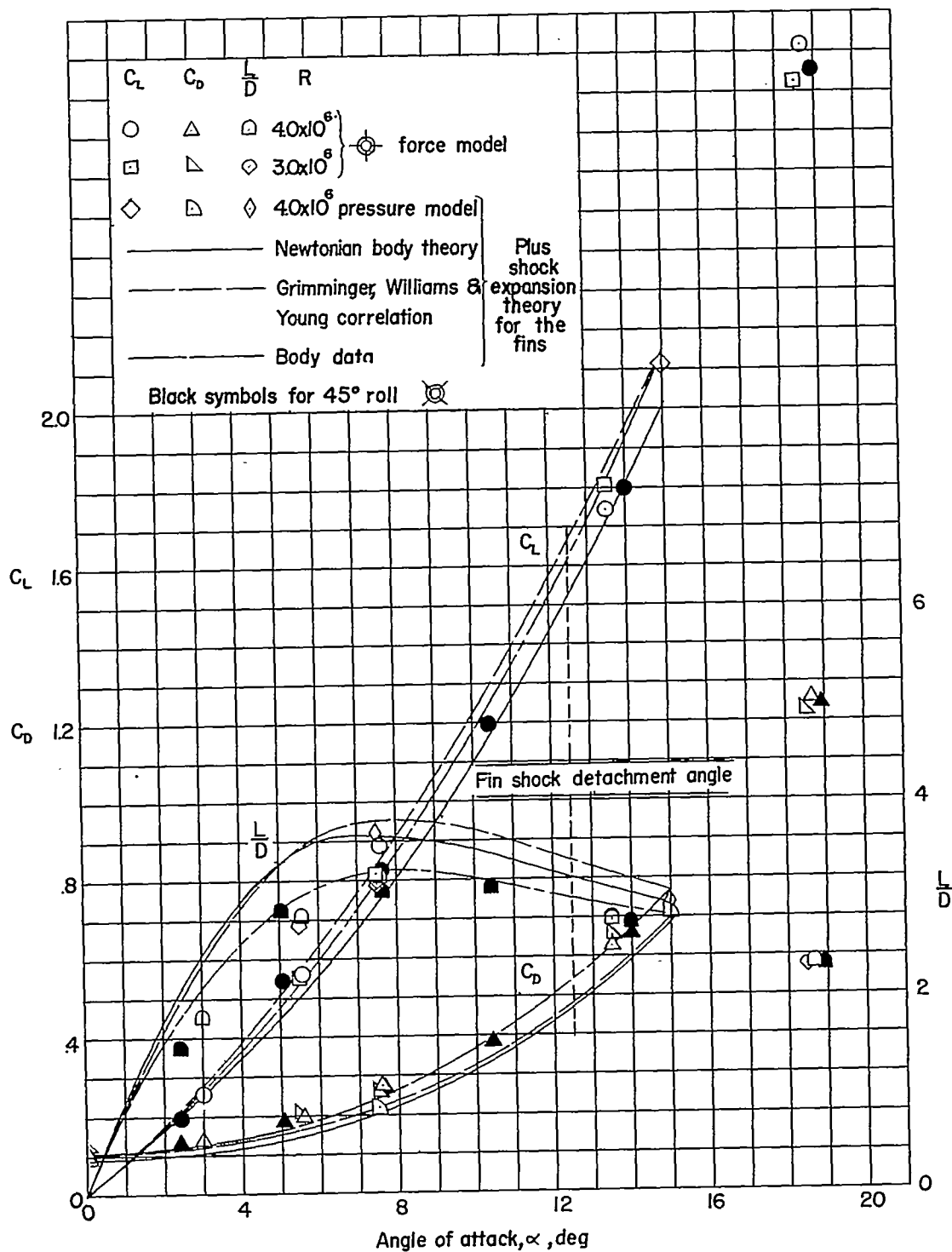
Figure 5.- Experimental and theoretical variation of lift coefficient, drag coefficient, and lift-drag ratio with angle of attack for the finned body at a Mach number of 6.9.
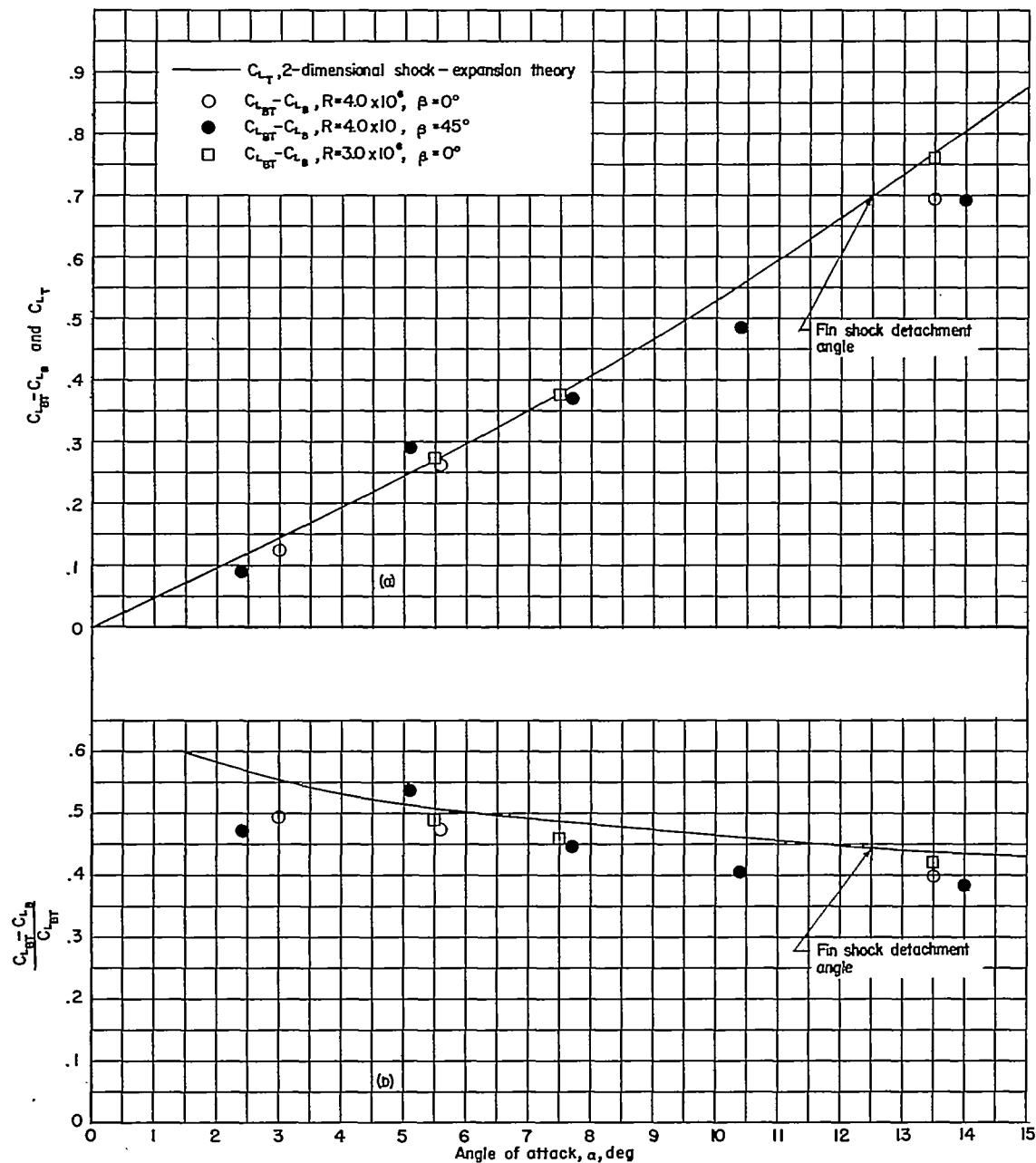
Figure 6.- Experimental and theoretical variation of the fin effectiveness with angle of attack for the finned body at a Mach number of 6.9.
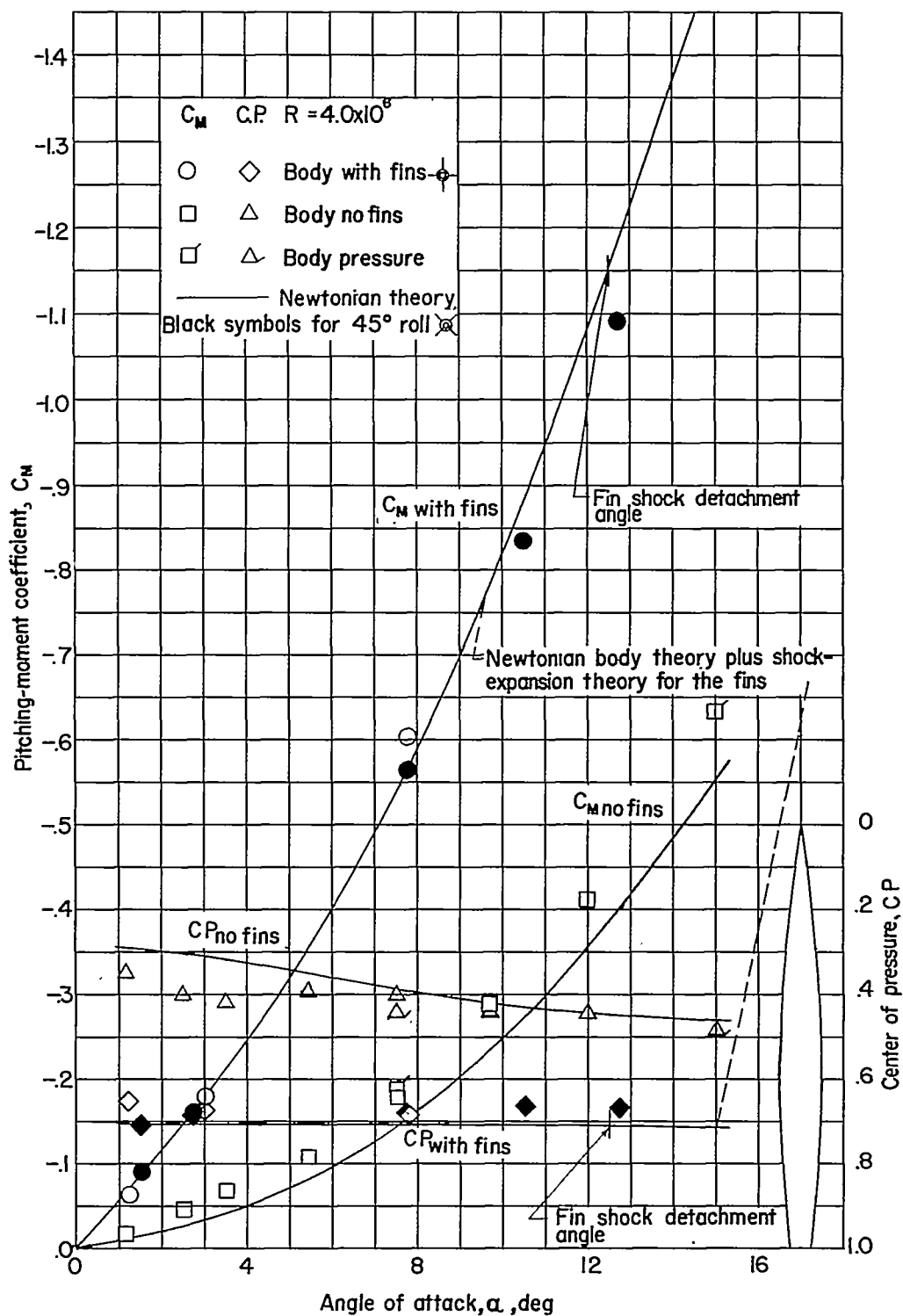
Figure 7.- Experimental and theoretical variation of the pitching-moment coefficient and center of pressure with angles of attack for the body alone and finned body at a Mach number of 6.9.
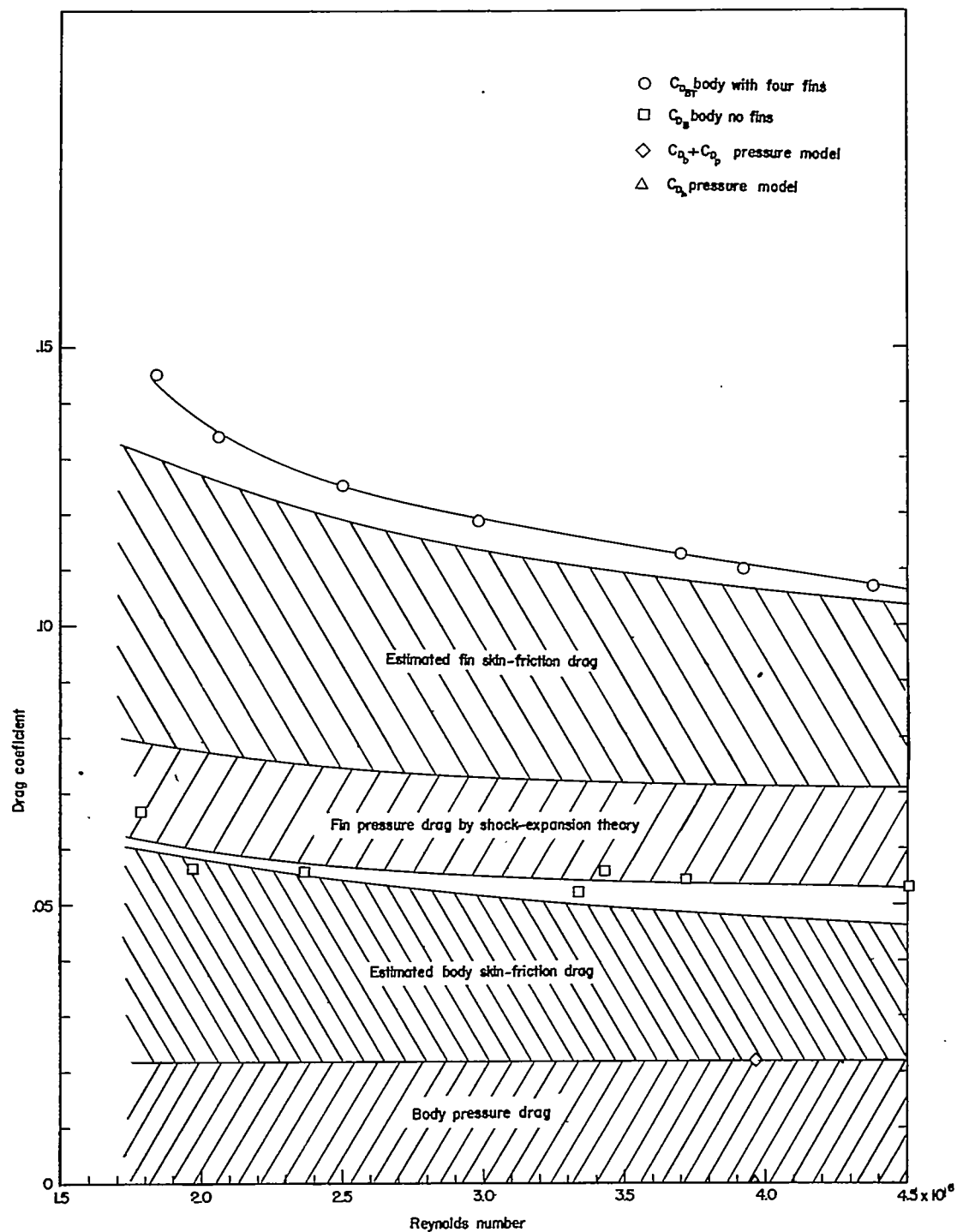
Figure 8.- Variation of the zero-lift components of drag with Reynolds number for the finned body at a Mach number of 6.9.
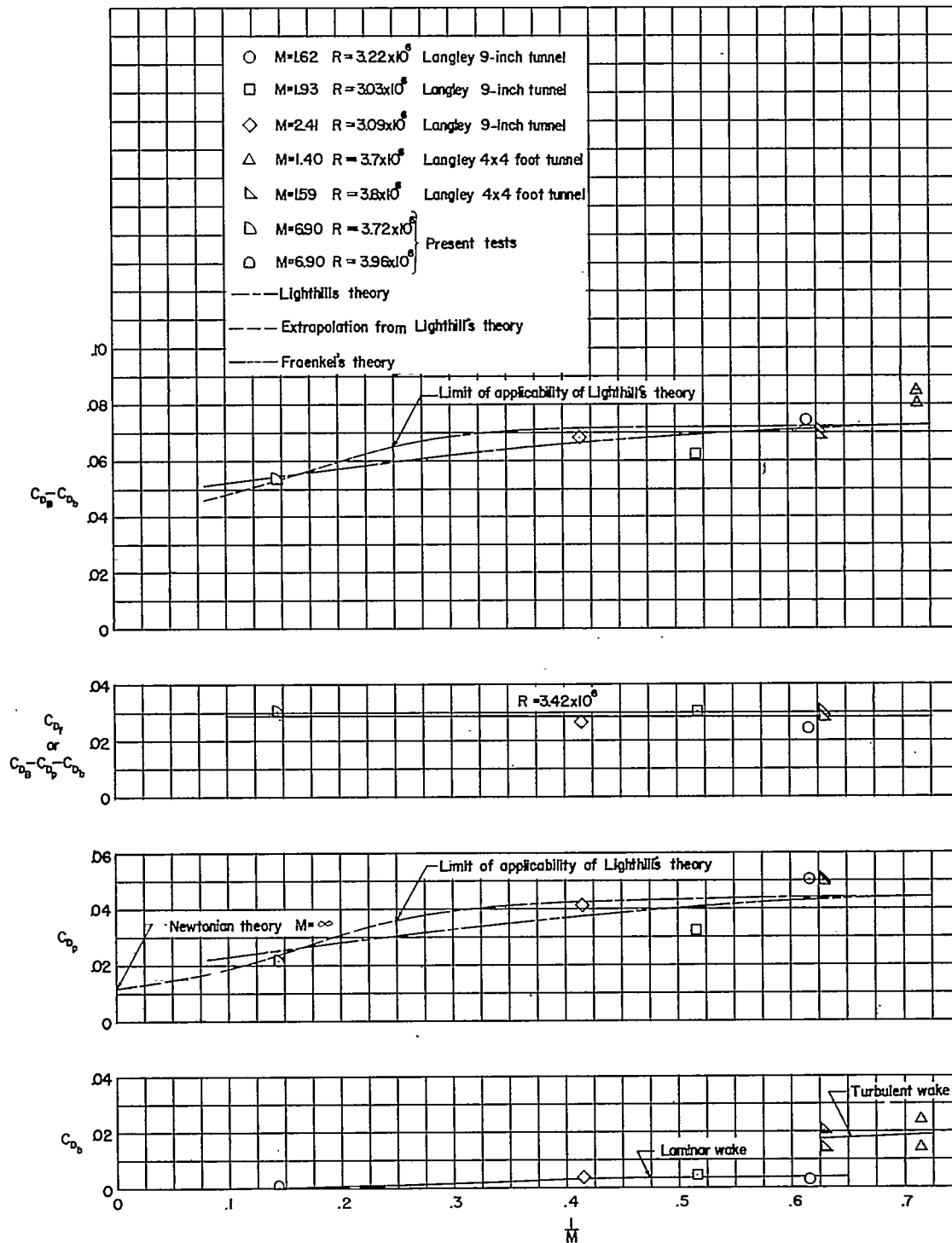
5K

Figure 9.- Variation of the zero-lift components of drag with the inverse
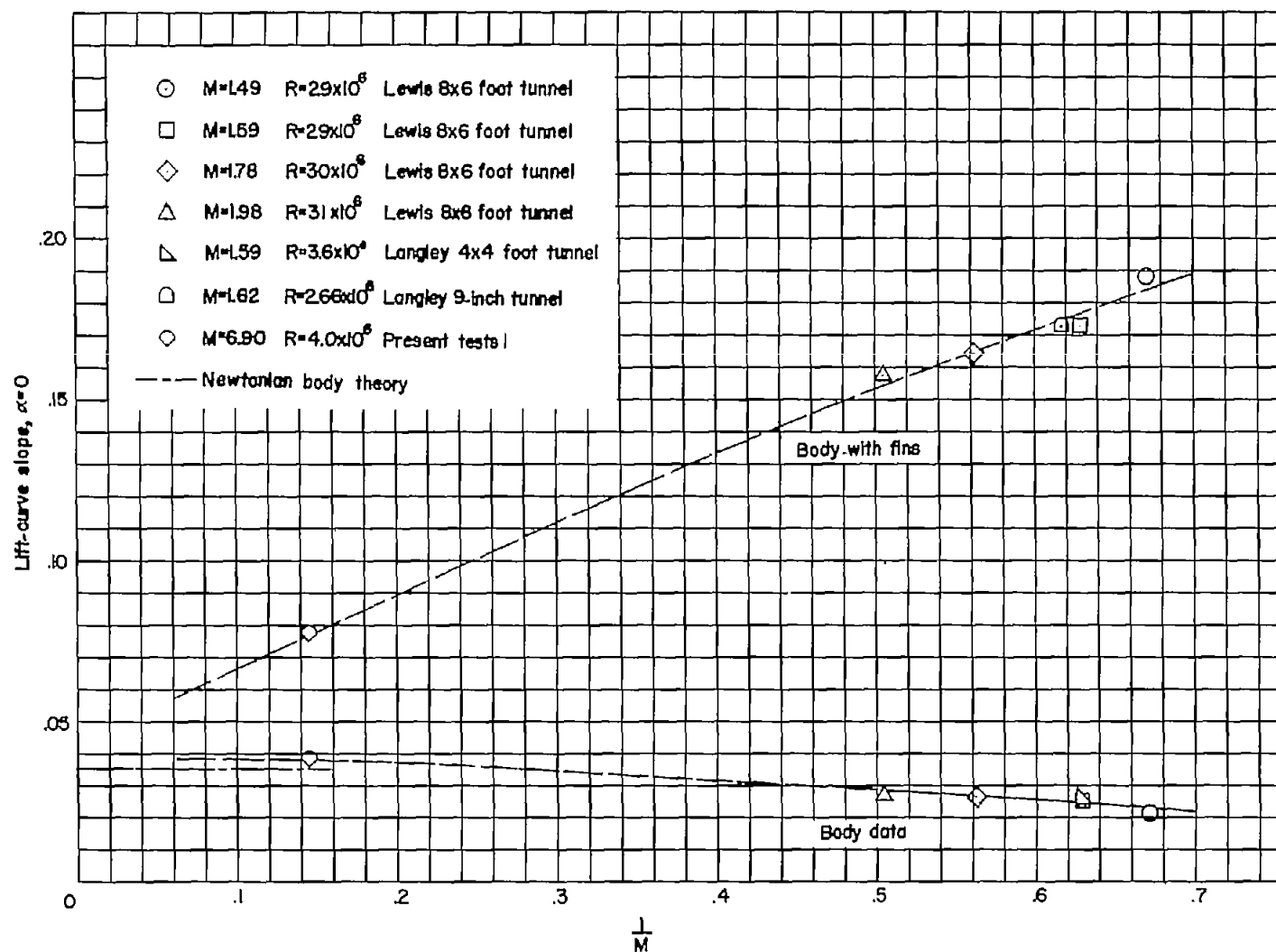Mach number for the body alone.

CONFIDENTIAL

Lift-curve slope, $\alpha = 0$

⊙	M=1.49	R=2.9x10⁶	Lewis 8x6 foot tunnel
□	M=1.59	R=2.9x10⁶	Lewis 8x6 foot tunnel
◇	M=1.78	R=3.0x10⁶	Lewis 8x6 foot tunnel
△	M=1.98	R=3.1x10⁶	Lewis 8x6 foot tunnel
◮	M=1.59	R=3.6x10⁶	Langley 4x4 foot tunnel
⎔	M=1.62	R=2.66x10⁶	Langley 9-inch tunnel
◯	M=6.90	R=4.0x10⁶	Present tests

— — — Newtonian body theory

.20

.15

.10

.05

Body with fins

Body data

0   .1   .2   .3   .4   .5   .6   .7

$\frac{1}{M}$

Figure 10.- Variation of the lift-curve slope at zero lift with the
inverse Mach number for the body alone and the finned body.
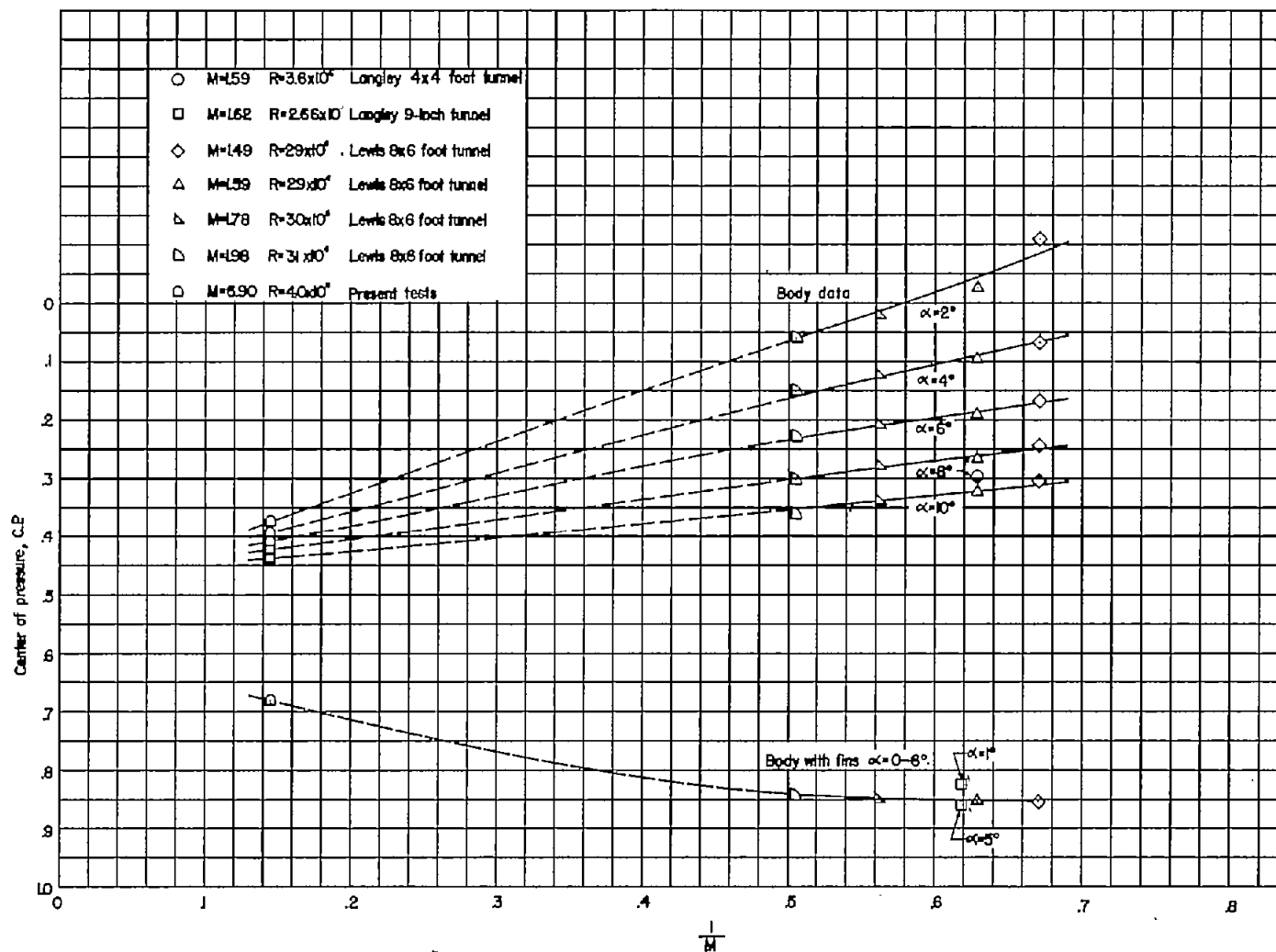
Figure 11.- Variation of the center of pressure with the inverse Mach
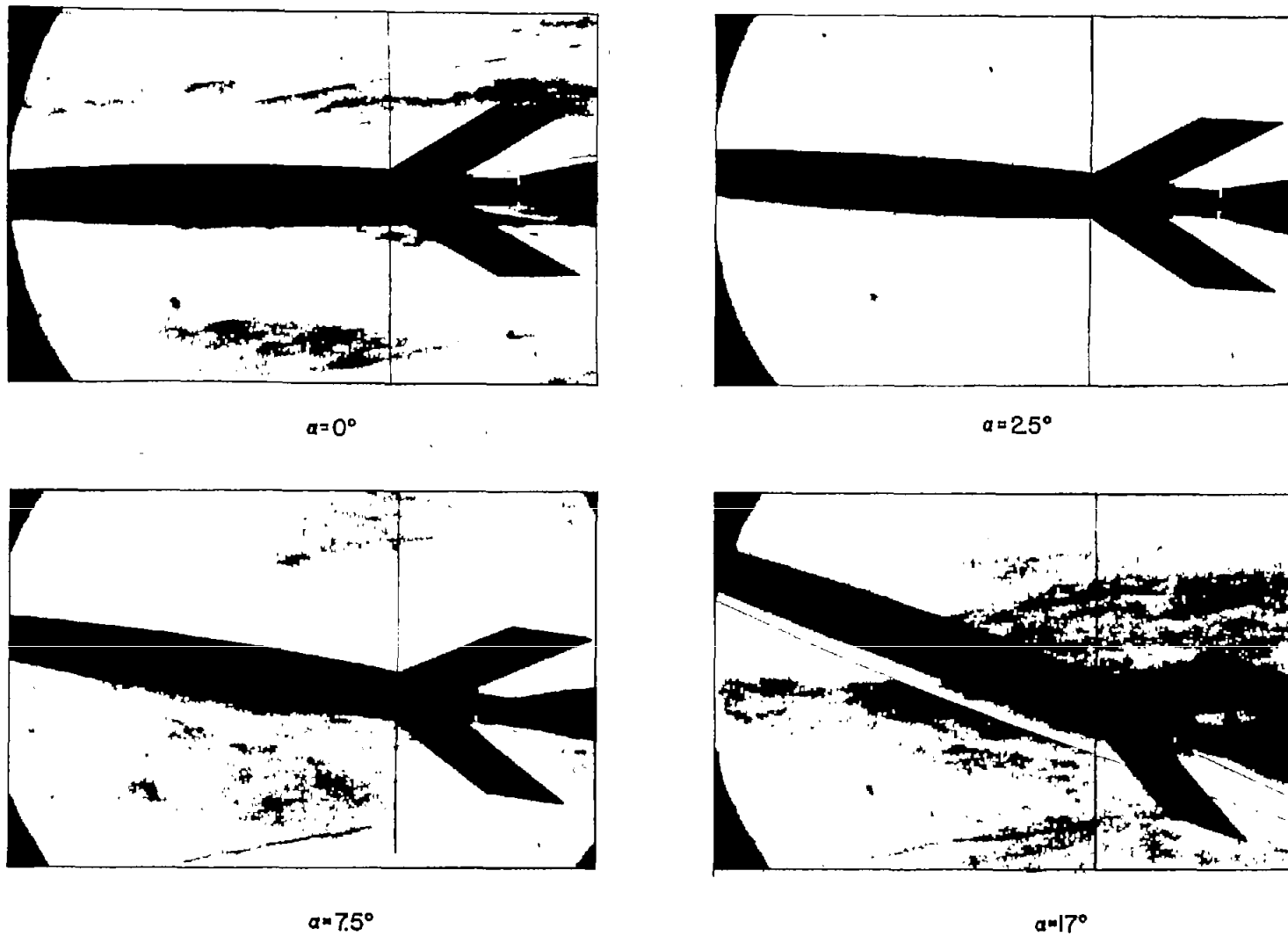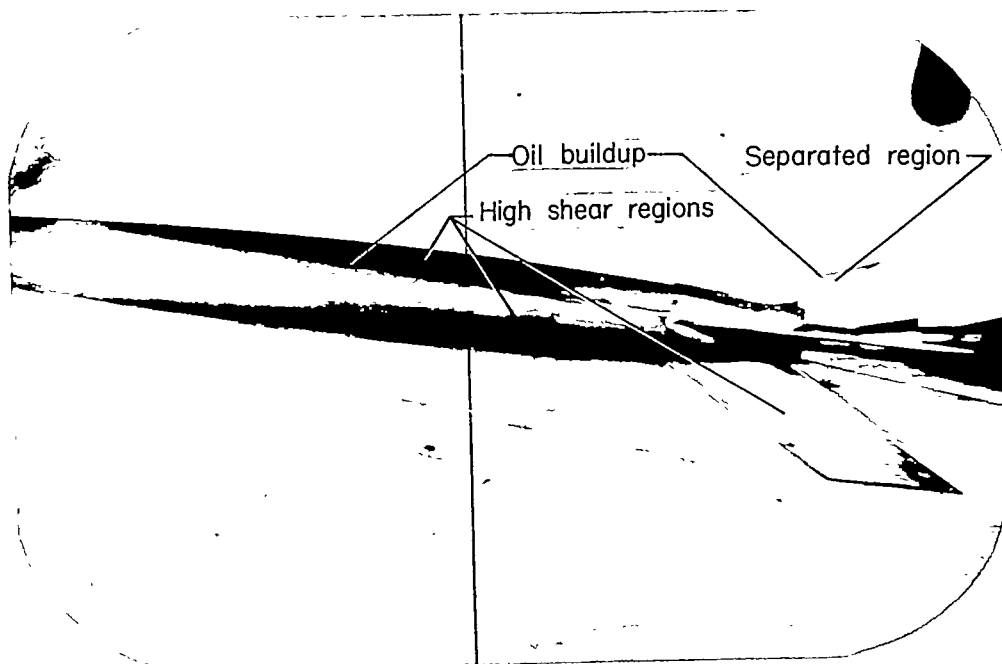number for the body alone and finned body.

a=0°

a=25°

a=7.5°

a=17°

Figure 12.- Schlieren photographs of shock wave and boundary-layer
variations with angle of attack at a Mach number of 6.9.
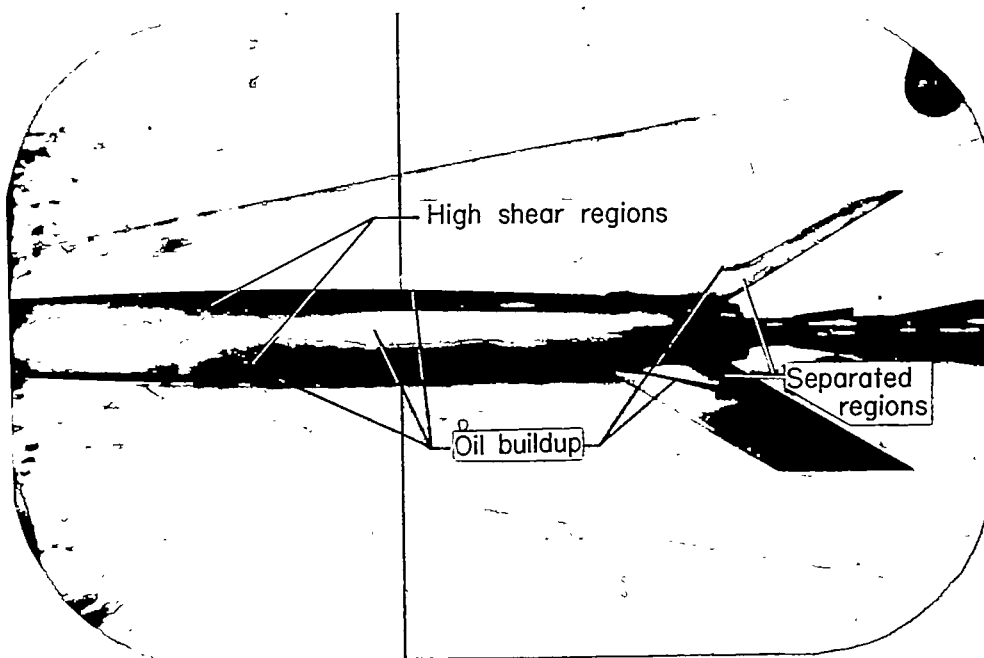
L-85652

Side view

Top view

L-85653.1

Figure 13.- Combination schlieren and fluorescent surface oil flow photographs for 7.5° angle of attack at a Mach number of 6.9.

NACA Res. Abst. , Aug. 24, 1955

Biva?/Beatrie M.2c

1 Mar. 5.6.